Characterisation of oxidised gadolinium film deposited on Si (1 0 0) substrate

A.A. Dakhel

Department of Physics, College of Science, University of Bahrain, P.O. Box 32038, Bahrain

Abstract

Thin Gd_2O_3 films were prepared by oxidation of Gd films grown on quartz and Si (P) substrates. The oxide films were characterised by X-ray fluorescence (XRF), X-ray diffraction (XRD), and optical absorption spectroscopy. The constructed $Al/Gd_2O_3/Si$ MOS devices were characterised by measurement of gate-voltage dependence of their capacitance and ac conductance, from which the surface states density (N_{ss}) of insulator/semiconductor (I/S) and the density of fixed charges in the oxide were determined. The electrical conduction and dielectric properties of the Gd_2O_3–Silicon structure were studied by ac and dc methods at room temperature and in the range of 293–343 K. The data of the ac measurements follow the correlated barrier-hopping (CBH) model and the data of the dc measurements obey the trap-charge-limited space-charge-limited conduction (TCLC–SCLC) mechanism. It was noticed that the total trap concentration (N_t) deduced from dc measurements has the same order of magnitude as the concentration of localized states (N_{LS}) extracted from ac measurements. The infrared studies informed us about the chemisorbed hydroxyl (OH) groups incorporation in the oxide film, which leave the freshly heated-treated film at 673 K.

© 2004 Elsevier B.V. All rights reserved.

Keywords: Insulating films; Gadolinium oxide; Dielectric phenomena; SCLC mechanism

1. Introduction

In recent years, rare earth oxides (REOs) have been used in the production of microcircuit elements, memory devices and sensors, as well as protective coating due to their appropriate physical properties [1]. They have high resistivity ($\rho = 10^{12}$–$10^{15}\ \Omega$ cm), high relative permittivity ($\varepsilon = 7$–20) and large band gap ($E_g = 4$–6 eV) [2]. Moreover, REOs are stable in contact with silicon at room temperature, but there is a possibility of formation of silicates during annealing at high temperatures (800–1000 °C) especially in oxygen or air atmosphere [3–6]. Most studies [6–11] were focused on pure REOs as insulators of a few-nanometres thickness for the production of a SiO_2-alternative or concentrated on investigation of the composition of the interface layer formed between REOs films and Si substrates.

Gadolinium oxide films grown on Si substrates were studied in several works [12–16]. They were prepared by different techniques, especially by electron-beam-gun (EBG) evaporation technique. The aim of the present investigation is to prepare Gd oxide films by oxidation of pure Gd films by means of annealing in air and to study their electrical properties, as well as to compare the results with those obtained for Gd_2O_3 films prepared by EBG evaporation method.

2. Experimental details

Thin film samples were deposited by evaporation of pure Gd in a vacuum system of about 10^{-3} Pa on Si and quartz substrates held at room temperature. The samples were oxidised by means of annealing in air in an oven at 400 °C for 15 min. For optical investigation, a cleaned quartz substrate was used and for electrical measurements, cleaned Si wafers (1 0 0) oriented and boron-doped with concentration of $1.2 \times 10^{22}\ m^{-3}$ were used. Wafers were thermo-chemically cleaned with 50%

potassium hydroxide (by weight) solution at 65 °C for 15 min. The MOS devices were made by deposition of aluminum films of about 150 nm to form gate and back contacts for each $Al/Gd_2O_3/Si$ (p)/Al structure. The samples were prepared simultaneously and their thickness was measured after annealing by Gaertner 117 ellipsometer of $\lambda = 632.8$ nm to be about 187.2 nm of refractive index about 2.09.

The composition of the oxide samples was studied by EDXRF method. The exciting X-ray beam from the Cu anode (35 kV and 40 mA) filtered by a Ni filter was incident on the film surface at 15°. The fluorescent yield was collected at 90° by using an Amptek XR-100CR, Si X-ray detector of energy resolution 180 eV at 5.9 keV. The crystal structure was investigated by a Philips PW 1710 X-ray diffractometer with Cu K_α radiation. The ac-measurements were performed using a Keithley 3330 LCZ instrument and hp 4275A LCR instrument (for 1 MHz measurements) with a signal of 50 mV. The dc measurements were done using a Keithley 614 electrometer. The FTIR spectra were recorded at room temperature in the range of 4000–200 cm^{-1} by using a Perkin-Elmer Spectrum-One FTIR spectrometer with a 16-scan number.

3. Gd-oxide film sample characterisation

3.1. Composition characterisation

Fig. 1 shows the X-ray fluorescence (XRF) spectrum of a Gd oxide film on Si substrate taken with an exposure time of 1 h. As seen, except signals from the Si substrate (1.74 keV for the K_α line) and Gd (6.05, 6.72, 7.10, and 7.78 keV for L_α, $L_{\beta 1}$, $L_{\beta 2}$, and $L_{\gamma 1}$, respectively) there are no other significant signals from the sample taking into consideration that the instrumental detection limit (IDL) [17] of the set-up used is about 800 ppm at an energy of about 5.84 keV.

The known method of micro-radiographic analysis [18,19] was used to study the concentration of Gd in the

prepared oxide films. The integrated intensity of the Gd L_α line from a standard sample and from the oxide film was measured. The standard sample was pure Gd_2O_3 powder submitted to a pressure of 750 MPa for 15 min, obtaining a pellet of about 2 mm thick. The used set-up sensitivity ($S_{Gd\,L_\alpha}$) for the Gd L_α was measured from the fluorescent integral intensity of Gd L_α line of the reference sample and using tables of mass absorption coefficient (μ_m) of Gd and O [20]. The self-absorption factor of the incident and fluorescent Gd L_α rays was calculated to be 0.91, which is near 1.0 for thin films as stated in ref. [19]. Then, the theoretical intensity of the Gd L_α line emitted from a pure Gd_2O_3 thin film of thickness 187.2 nm was calculated to be (520E$-3 \pm$ 5.4E-3 cps), while the direct experimental value was (508E$-3 \pm$ 11E-3 cps). It is clear that the results are very close to one another within the experimental error. Hence, the evaporated films have the content of Gd_2O_3. This conclusion is supported by X-ray diffraction (XRD). But, the stoichiometry of the samples can be determined accurately if the oxygen composition is analysed, that cannot be done with the used detector.

3.2. Structural characterisation

Fig. 2 presents the XRD of Gd_2O_3 powder as a reference. It shows a C-type cubic structure with $a = 1.083$ nm, which is close to the published value [21]. XRD of the film grown on Si (1 0 0) substrate shows a polycrystalline C-type Gd_2O_3 structure. The average grain size calculated by the Scherrer formula [22] from the most intense (2 2 2) line was about 23 nm. The film has [1 0 0] preferred orientation as deduced from the comparison of the relative intensities of (2 2 2), (4 0 0), and (4 4 0) reflections from the film sample with those from the random distributed fine grains in pure Gd_2O_3 powder. This film orientation takes place due to exchange orientation as a result of lattice match ($a_{Gd_2O_3} = 1.083$ nm and $2a_{Si} =$
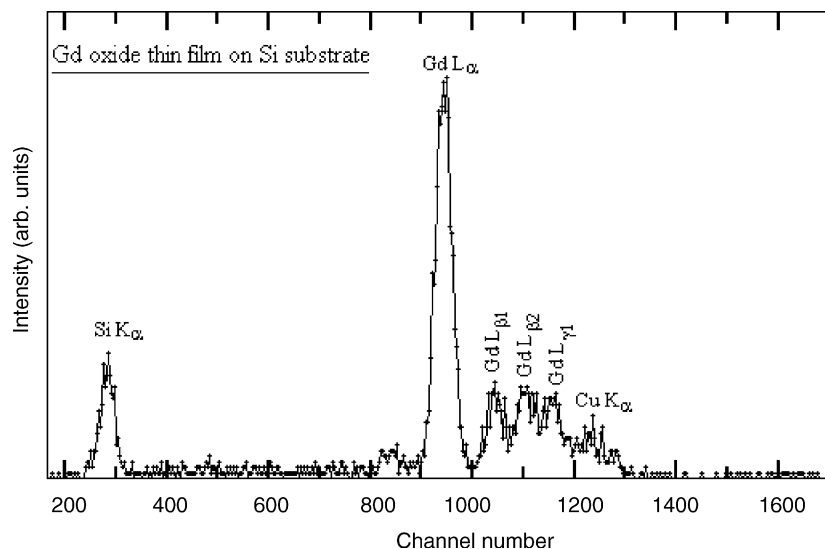

Fig. 1. XRF spectrum of gadolinium oxide film grown on Si substrate. The exciting line is Cu K_α line of energy 8.047 keV.
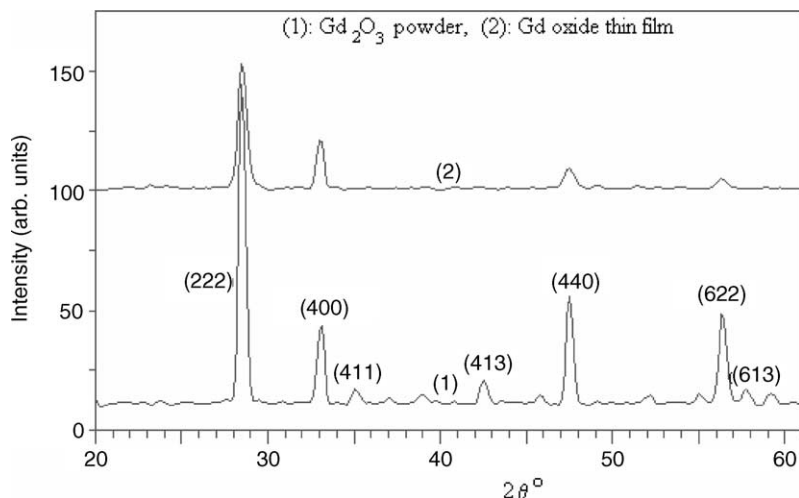
Fig. 2. X-ray diffraction of Gd_2O_3 powder and Gd oxide film sample. The shown patterns were obtained from smoothed data SM-files and the scan speed was 0.01°/s.

1.086 nm) of the Si (1 0 0) substrate and the overgrown film during its crystallization.

3.3. UV–vis optical characterisation

The spectral normal transmittance of a polycrystalline Gd_2O_3 film grown on quartz substrate in the transparent and absorption regions (200–1100 nm) is shown in Fig. 3 with interference fringes. The transmittance data were corrected relative to the optically identical uncoated substrate. The investigated sample has high transparency $T > 0.90$ in the transparent region and a sharp absorption edge that is attributed

to the direct transitions [23]. The energy gap was calculated according to the method discussed in ref. [24] to be 6.2 eV. This value is different from the value (5.2 eV) reported in ref. [25]; the energy 5.2 eV in the present work represents the beginning of the transparent region.

4. Ac and dc measurements

4.1. Characterisation of MOS structure

Fig. 4 shows the bias-voltage dependence of the capacitance $C(V_g)$ and ac-conductance $G(V_g)$ measured at 1 MHz
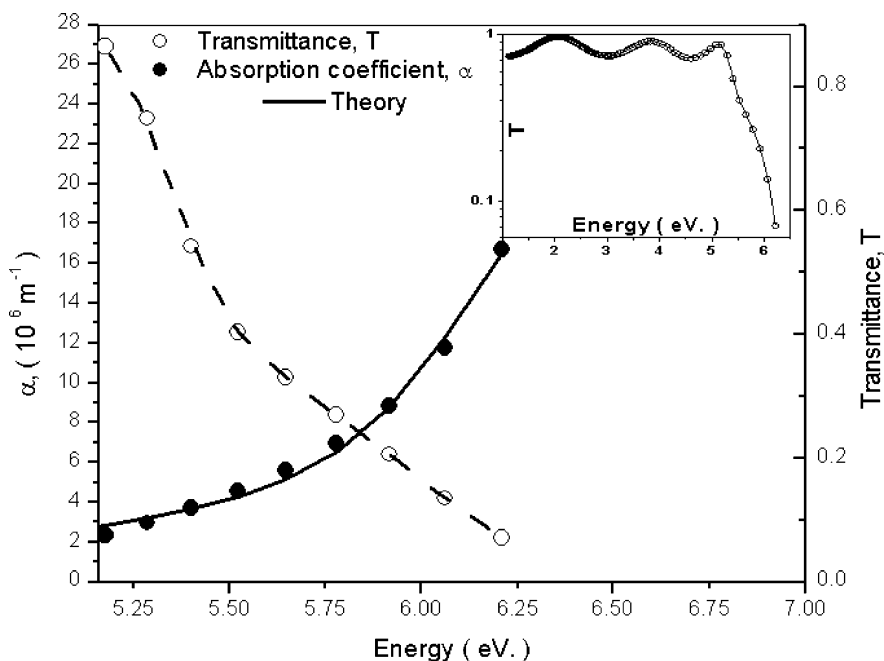

Fig. 3. Normal spectral transmittance $T(E)$ and absorption coefficient $\alpha(E)$ of polycrystalline Gd_2O_3 film grown on quartz substrate in the fundamental absorption region. The inset shows the complete spectral normal transmittance.
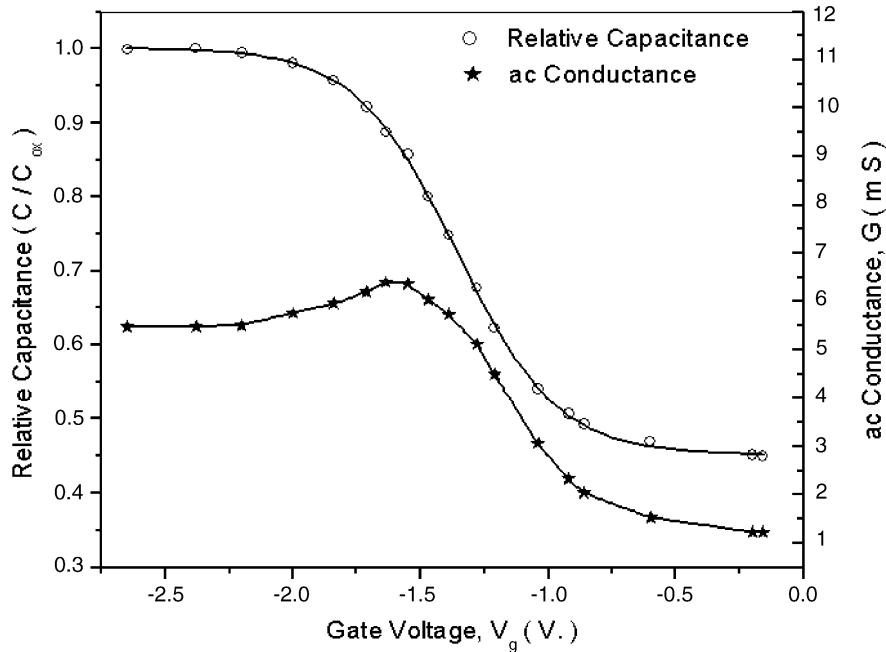
Fig. 4. Gate-voltage dependence of the capacitance $C(V_g)$ and conductance $G(V_g)$ measured at 1 MHz for (Al/Gd$_2$O$_3$/Si/Al) MOS device at room temperature. The measuring signal was 50 mV.

and room temperature using a parallel circuit mode. These curves have the ordinary form of a MOS structure. The relative permittivity ε_{ox} of the insulator can be calculated from the accumulation capacitance per unit area C'_{ox} at 1 MHz [26,29]: $C'_{ox} = \varepsilon_o \varepsilon_{ox}/d$, where ε_o is the permittivity of vacuum and d is the film thickness. The result is $\varepsilon_{ox} = 7.5$, which is low compared to the value 16 obtained in ref. [13] for Gd$_2$O$_3$ films prepared by EBG evaporation technique on Si substrates or the value of about 10 of ref. [14]. It is possible to consider the calculated value of ε_{ox} as an effective value due to the formation of a very thin SiO$_2$ interfacial layer of effective thickness 1–2.5 nm [13,27] as a result of the 400 °C annealing. Consequently, one needs to correct the measured relative permittivity using the model of two "in series-connected capacitors" [28]: $\{\varepsilon_m^{-1} = \varepsilon_{corr}^{-1} + (t_{SiO_2}/\varepsilon_{SiO_2})d^{-1}\}$, where $\varepsilon_m = 7.5$, $t_{SiO_2} = 2.5$ nm, $\varepsilon_{SiO_2} = 3.82$ and $d = 187.2$ nm, we find $\varepsilon_{corr} = 7.7$. But this correction is not significant, so that one cannot explain the obtained low value of ε_{ox} by only the formation of an interfacial thin layer of SiO$_2$. Rather one has to conclude that the Gd oxide itself, prepared by the present-work method, has low relative permittivity relative to that value obtained for Gd$_2$O$_3$ film prepared by EBG evaporation technique. It was reported in ref. [29] that the oxidation of Gd in air is accompanied by a slow replacement of O by OH. This point may possibly explain the situation and therefore one needs to study it by FTIR spectroscopy, as in Section 5. Generally, it is clear that the preparation of Gd$_2$O$_3$ in the present method cannot produce an insulator, which might be considered as high-k dielectric in MOS applications as that prepared by the EBG method.

The flat-band voltage (V_{FB}) of the $C–V_g$ curve at 1 MHz is about -1.5 V. Consequently, the density per unit area of

the charges in the oxide can be calculated by the following equation [30]:

$$Q_{ox} = \left(\frac{C'_{ox}}{e}\right)(\Phi_{ms} - V_{FB}) \qquad (1)$$

where $C'_{ox} = C_{ox}/A$ is the capacitance per unit area of the oxide insulator, e is the electronic charge and $\Phi_{ms} = -0.9$ V is the work-function difference between Al gate and silicon substrate [26]. The result is 1.3×10^{15} charges/m^2 (or the Q_{ox}/d $= 8.2 \times 10^{21}$ charges/m^3). These mainly fixed charge-centres are created due to oxygen-vacancies and various types of defects and impurities and hence, their concentration depends on the annealing parameters.

The interface trap density N_{ss} at Si midgap is determined from the combination of a single high-frequency (1 MHz) $C(V_g)$ and $G(V_g)$ characteristics using Hill's method [31]:

$$N_{ss} = \frac{2}{eA} \frac{(G_{max}/\omega)}{[(G_{max}/\omega C_{ox})^2 + (1 - C_m/C_{ox})^2]} \qquad (2)$$

where G_{max} is the maximum measured conductance in the $G–V_g$ plot of Fig. 4 with its corresponding measured capacitance C_m. The result of calculation of N_{ss} is about 1.4×10^{16} eV^{-1}/m^2, which is not high enough to pin the Fermi level of the Si substrate. Consequently the interface traps and defects cannot prevent the construction of an MOS device.

4.2. AC conduction measurements

4.2.1. Theoretical

The ac conductivity consists of two contributions according to the following relation: $\sigma_{ac} = \sigma_{dc}(0) + \sigma_{ac}(\omega)$ [32],

where $\sigma_{dc}(0)$ is the dc conductivity extrapolated to zero-frequency and $\sigma_{ac}(\omega)$ is a frequency-dependent part of the conductivity. In the present investigation, a suitable theoretical model to study the function $\sigma_{ac}(\omega)$ is the correlated barrier-hopping (CBH) model [33,34]:

$$\sigma_{ac}(\omega) = \frac{n_{el}\pi^3}{24} N_{LS}^2 \varepsilon_o \varepsilon_{ox} \omega R_\omega^6 \tag{1a}$$

where N_{LS} is the concentration of localized states near the band edge, $\varepsilon_o\varepsilon_{ox}$ is the insulator permittivity, and R_ω is the hopping distance given by:

$$R_\omega = \frac{n_{el}e^2}{\pi\varepsilon_o\varepsilon[W_M + k_B T \ln(\omega\tau_o)]} \tag{2a}$$

where W_M is the effective hopping barrier and τ_o is the effective relaxation time (approximately 10^{-13} s according to [35]), n_{el} is the number of simultaneously hopped electrons. The conductivity $\sigma_{ac}(\omega)$ can be expressed in form of a power law: $\sigma_{ac}(\omega) = A_\sigma\omega^s$, where A_σ is the pre-exponential and s is the exponent given by [33]:

$$s = 1 - \frac{6k_B T}{W_M + k_B T \ln(\omega\tau_o)} \tag{3}$$

4.2.2. Experimental

The frequency dependence of the capacitance $C(\omega)$ and ac-conductivity $\sigma_{ac}(\omega)$ of the MOS structure were measured at an accumulation bias voltage (-2.5 V) under which the $C(\omega)$ and $\sigma_{ac}(\omega)$ characteristics are determined mainly by the capacitance and the ac-conductivity of the insulator layer. Fig. 5 shows the dependence $C(\omega)$ and $\sigma_{ac}(\omega)$ at room temperature in the frequency range of 5–100 kHz. The calculation shows that the CBH model (and consequently the power law) is convenient to describe these experimental data. The values of s and W_M at room temperature are: 0.97 and 6.2 eV, respectively. The value of W_M is equal to the energy gap and satisfies Eq. (3). The minimum hopping distance [36] $R_{min} = [e^2/\pi\varepsilon_o\varepsilon W_M]$ is 0.2 nm. The value of $\sigma_{dc}(0)$ is 4.1×10^{-6} S/m, which is almost equal to the dc conductivity (3.1×10^{-6} S/m) measured by dc method at $V_g = -2.5$ V. The fitting of the experimental data to Eq. (1) gives the value of αN_{LS} (where the parameter $\alpha = n_{el}^{7/2}$) to be 1.4×10^{28} m^{-3}. We mention that the calculated value of the exponent s suggests that the conduction in the present case is not based on the quantum mechanical tunnelling (QMT) model for which $s \approx 0.8$ [37].

The capacitance decreases with increasing signal frequency. This dispersion can be attributed basically to the effect of charge redistribution by carrier hopping on centres [38]. However, it was proved by Kramers–Kronig (KK) relations [39–41] that the power law of ac conductivity of an insulator causes the permittivity (or capacitance) to follow the relation [32]:$C(\omega) \propto \omega^{s-1}$. As seen from Fig. 5, this relation is adequate for frequencies $f > 10$ kHz.

4.2.3. Effect of temperature

It was found in the present work that the value of s is almost not varying with temperature in the range of 293–343 K. But, the temperature dependence of the capacitance of the insulator/Si structure at 100 kHz is shown in Fig. 6. The capacitance decreases with increasing of temperature. The temperature coefficient of the capacitance TCC is about -8×10^{-3} K^{-1} at 300 K.

4.3. DC electrical measurements

4.3.1. Theoretical

Several different mechanisms have been proposed to explain the current transfer in insulators [26]. The mechanism which a certain I–V characteristics should follow depends on the sample structure and trap concentration, and hence on the conditions and method of preparation. The experimental data refer to Poole–Frenkel (PF) and space-charge-limited current (SCLC) mechanisms.

The relationship between the current density J and the applied voltage V at temperature T according to PF mechanism is given in refs. [26,42]:

$$J = A_{PF}V\exp\left\{e\frac{(\beta_{PF}V^{1/2}/d^{1/2} - \Phi_{PF})}{k_B T}\right\} \tag{3a}$$

where A_{PF} is a pre-exponential factor, Φ_{PF} is the PF barrier height, and β_{PF} is a field lowering coefficient, which is given by $\beta_{PF} = (e^3/\pi\varepsilon_o\varepsilon_{ox})^{1/2}$.

The trap-charge-limited space-charge-limited conductivity (TCLC–SCLC) mechanism describes the restriction of the current flow in a dielectric material by the density of free injected carriers and trap concentration [43]. The relationship between current density and applied voltage is given by $J \sim V^n$, where n is an exponent determined by the energy distribution of traps within the forbidden band of the insulator: $n = 2$ for traps of a discrete single localised energy level [44,45] and $n > 2$ for exponential distribution of trap levels [46]. Data of the present investigation follow the TCLC–SCLC mechanism with $n > 2$ for which the following relation is satisfied [47,48]:

$$J = e\mu N_c\left(\frac{\varepsilon_{ox}\varepsilon_o}{eN_0 k_B T_t}\right)^\iota \frac{V^{\iota+1}}{d^{2\iota+1}} \tag{4}$$

where N_c is the effective density of states in the conduction band and μ is the carrier mobility. $\iota = T_t/T = n - 1$, and T is the absolute temperature. T_t is a temperature parameter related to the exponential trap distribution $N(E)$ as $N(E) = N_0\exp(-E/k_B T_t)$, where N_0 is the value of $N(E)$ at the conduction band-edge. The total traps concentration is given by $N_t = N_0 k_B T_t$ [49]. The value of N_t can be determined from the experimental measurements of dc J as a function of T at accumulation polarity. The relation between Ln(J) and $1/T$ is
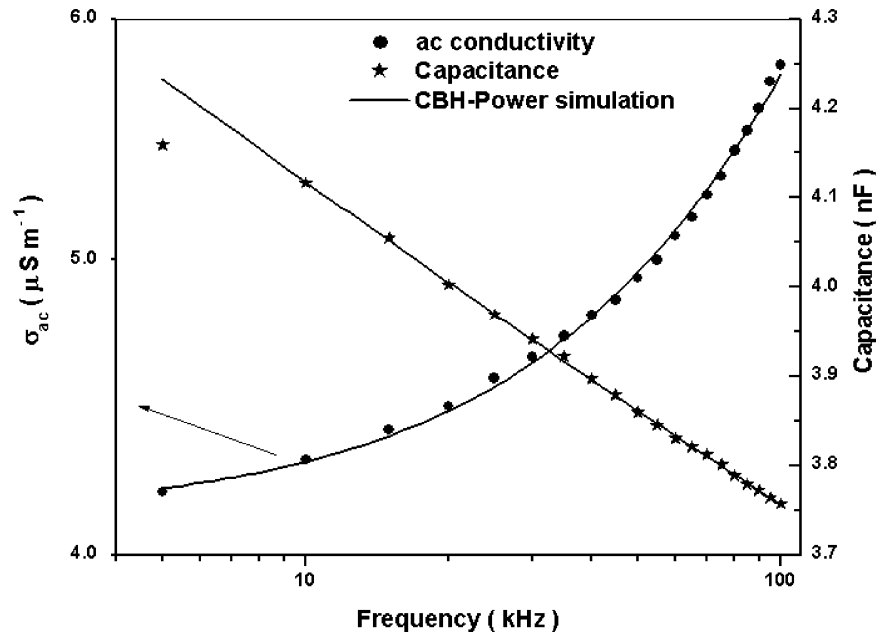
Fig. 5. Frequency dependence of the capacitance $C(\omega)$ and ac-conductivity $\sigma_{ac}(\omega)$ measured at room temperature under accumulation voltage ($V_g = -2.5$ V) for Gd$_2$O$_3$ film grown on Si substrate. The lines represent the theoretical calculation according to Elliott CBH model and KK model.

linear of slope s given by [48]

$$s = T_t \mathrm{Ln}\left(\frac{\varepsilon_0 \varepsilon_{ox} V_g}{e N_t d^2} \right) \qquad (5)$$

4.3.2. Experimental

The gate-voltage and temperature dependence of the current density ($J(V)$ and $J(T)$) of the (insulator–Si) structure were measured at the accumulation mode of the p-type Si substrate, in which the $J(V)$ and $J(T)$ curves are determined mainly by the conductivity of the insulator layer [50]. The dependence of leakage current density J per unit voltage on root of gate voltage V_g (the PF-plot) at the accumulation mode at 293 K is depicted in Fig. 7. It is clear that the data are not following the PF mechanism. Meanwhile, the log–log plot of the leakage current density J as a function of gate voltage at accumulation mode at 293 K is straight line. This means
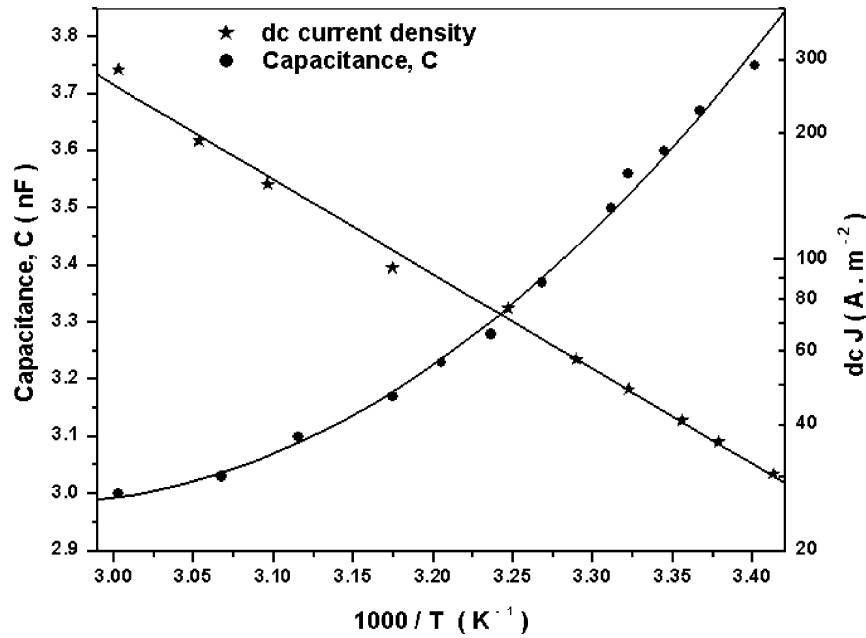

Fig. 6. Arrhenius plot of temperature dependence of the dc leakage current density under accumulation voltage ($V_g = -2.5$ V) and the temperature dependence of the capacitance of the MOS device at 100 kHz.
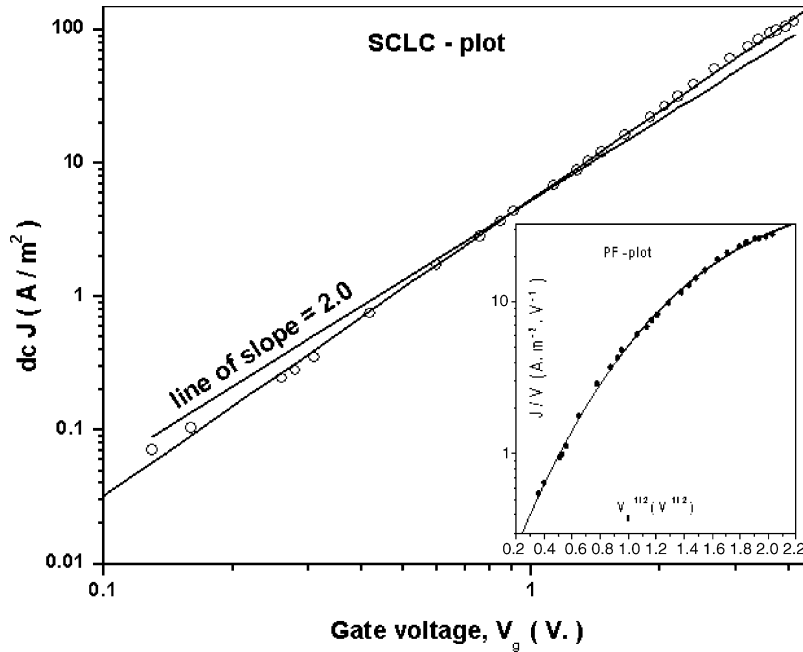
Fig. 7. Gate-voltage dependence of dc current in MOS device. The data follow the TCLC–SCLC mechanism. The inset shows the PF plot.

that data follow the TCLC–SCLC mechanism with $n = 2.22$. The value of N_t can be found from the measured relative permittivity $\varepsilon_{ox} = 7.5$ and the linear relationship between $\mathrm{Ln}(J)$ and $1/T$ in the range 293–343 K under an accumulation voltage ($V_g = -2.5$ V), which is shown in Fig. 6 with s equal to -5135.3 K. Thus, the results of TCLC–SCLC data-analysis are $N(E) = 1.1 \times 10^{49} \exp(-32.5\,E(\mathrm{eV}))\,\mathrm{J}^{-1}/\mathrm{m}^3$ and $N_t = 5.1$

$\times 10^{28}\,\mathrm{m}^{-3}$. The order of magnitude of N_t is the same as that of the concentration of the localised states N_{LS} calculated from ac measurements for one-electron hopping. This is an expected result as long as both N_t and N_{LS} refer to the same trap concentration in the energy gap of the insulator. Such result was observed in the work of ref. [51] on silicon nitride thin films.
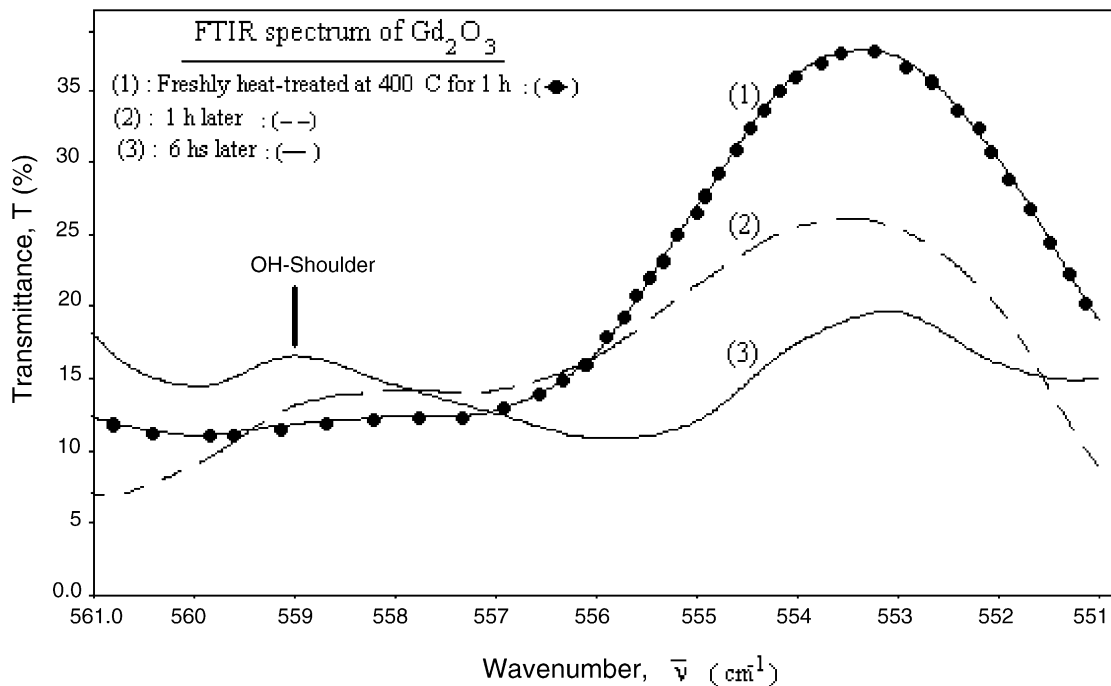

Fig. 8. The FTIR spectrum of Gd_2O_3 thick film sample in three modes; (1): freshly heat-treated at 400 °C for 1 h, (2): after 1 h, and (3): after 6 h being in air atmosphere.

5. FTIR absorption spectroscopy

As mentioned in Section 4.1, one of the reasons for the lowering of the relative permittivity of the prepared Gd_2O_3 oxide film might be the structural content of the film itself, especially the humidity incorporated in the oxide. Therefore, we have studied the FTIR spectrum of a thick Gd_2O_3 film. The spectrum did not show any distinct peak in the range of 3550–3200 cm^{-1}, which corresponds to the absorption of the adsorbed lattice-water molecules (or symmetric and anti-symmetric OH stretching). Also the spectrum did not show any distinct peak in the range of 1630–1600 cm^{-1} that corresponds to HOH bending (or OH deformation vibration "δ") [52]. Thus, it is possible to postulate that the humidity-incorporation is in a form of chemisorbed hydroxyl groups, as postulated in [53–55] and found experimentally in the work of ref. [29], which studied the oxidation of thin Gd films by XPS. Consequently, the FTIR study has focused on the vicinity of the absorption band of Gd_2O_3, which is around 559 cm^{-1} as reported in refs. [16,56,57] and graphically recorded in ref. [58]. The OH incorporation appears in the details of Fig. 8, which shows the IR spectra taken at room temperature for thick Gd_2O_3 film in three states: freshly heated-treated at 400 °C for 1 h, after 1 h, and after 6 h being in air atmosphere in order to observe the progress of the OH incorporation effect on the FTIR spectrum. As seen from Fig. 8, the freshly heat-treated oxide did not show any peak or feature in the Gd–O absorption band in the band 561–556 cm^{-1}. The OH-feature or peak appears gradually with the "aging" of the film in air atmosphere. These chemisorbed hydroxyl (OH) groups leave the film completely at high temperatures (673 K). Therefore, we conclude that the chemisorbed hydroxyl groups incorporation in the oxide film might be one of the reasons for lowering the value of measured relative permittivity.

6. Conclusion

In the present work, polycrystalline Eu_2O_3 films were prepared on quartz and Si (P) substrates by oxidation of Gd films. The constructed Al/oxide/Si MOS devices were characterised by the measurement of the gate voltage dependence of their capacitance and ac-conductance. The oxide film was characterised by XRF, XRD, and UV–vis optical spectroscopy. It was found that the prepared oxide has C-type structure with an energy gap of 6.2 eV. Ac and dc measurements were done for the prepared oxide films. The data of the ac measurements follows the correlated barrier-hopping model and the data of the dc measurements obey the trap-charge-limited space-charge-limited conductivity mechanism. It was noticed that the total trap concentration (N_t) extracted from dc measurements is of the order (10^{28} m^{-3}), which is the same order as magnitude of the concentration of localized states (N_{LS}) near the band edge as deduced from ac measurements. The FTIR studies informed us about the humidity incorporation in the oxide film in form of chemisorbed hydroxyl (OH) groups that leave the freshly heated-treated film at 673 K. This hydroxyl incorporation might be one of the reasons for the low value of the relative permittivity (7.5) of the oxide film measured at 1 MHz.

References

[1] T. Wiktorczyk, J. Electrostatics 51–52 (2001) 131.
[2] V.A. Rozhkov, A.Yu. Trusova, I.G. Berezhnoy, Thin Solid Films 325 (1998) 151.
[3] Z.M. Wang, J.X. Wu, M.S. Ma, W. Chen, Q. Fang, J.-Y. Zhang, Microelectron. Eng. 66 (2003) 608.
[4] H. Nohira, T. Shiraishi, T. Nakamura, K. Takahashi, M. Takeda, S. Ohmi, H. Iwai, T. Hattori, Appl. Surf. Sci. 216 (2003) 234.
[5] L. Kepinski, M. Wolcyrz, M. Marchewka, J. Solid State Chem. 168 (2002) 110.
[6] H.J. Osten, E. Bugiel, A. Fissel, Solid-State Electron. 47 (2003) 2161.
[7] A. Fissel, J. Dabrowski, H.J. Osten, J. Appl. Phys. 91 (2002) 8986.
[8] J. Kwo, M. Hong, A.R. Kortan, K.L. Queeney, Y.J. Chabal, R.L. Opila Jr., D.A. Muller, S.N.G. Chu, B.J. Sapjeta, T.S. Lay, J.P. Mannaets, T. Boone, H.W. Krautter, J.J. Krajewski, A.M. Sergent, J.M. Rosamilia, J. Appl. Phys. 89 (2001) 3920.
[9] G.L.P. Berning, H.C. Swart, Surf. Interface Anal. 26 (1998) 420.
[10] A.A. Dakhel, J. Alloys Compd. 365 (2004) 233.
[11] J.A. Gupta, D. Landheer, G.I. Sproule, J.P. McCaffrey, M.J. Graham, K.-C. Yang, Z.-H. Lu, W.N. Lennard, Appl. Surf. Sci. 173 (2001) 318.
[12] C. Ohshima, I. Taguchi, I. Kashiwagi, H. Yamamoto, S. Ohmi, H. Iwai, Appl. Surf. Sci. 216 (2003) 302.
[13] D. Landheer, J.A. Gupta, G.I. Sproule, J.P. McCaffrey, M.J. Graham, K.-C. Yang, Z.-H. Lu, W.N. Lennard, J. Electrochem. Soc. 148 (2) (2001) 29.
[14] M. Hong, J. Kwo, A.R. Kortan, J.P. Mannaerts, A.M. Sergent, Science 283 (5409) (1999) 1897.
[15] Y. Jun-Kyu, K. Min-Gu, P. Hyung-Ho, Thin Solid Films 420421 (2002) 571.
[16] H. Guo, X. Yang, T. Xiao, W. Zhang, L. Lou, J. Mugnier, Appl. Surf. Sci. 230 (2004) 215.
[17] R.M. Rousseau, Rigaku J. 18 (2001) 33.
[18] M.J. Anjos, R.T. Lopes, E.O.F. de Jesus, R. Cesario, C.A.A. Barradas, Spectrochem. Acta B 55 (2000) 1189.
[19] S. Hayakawa, J. Xiao-Peng, M. Wakatsuki, Y. Gohshi, T. Hirokawa, J. Cryst. Growth 210 (2000) 388.
[20] S. Sasaki, X-ray Absorption Coefficients of the Elements, National Laboratory of High Energy Physics, Oho 1-1, Tsukuba 305, Japan, 1990.
[21] J.C. Bailer (Ed.), Comprehensive Inorganic Chemistry, Pergamon Press Ltd., Oxford, 1973.
[22] E.F. Kaelble (Ed.), Handbook of X-rays for Diffraction, Emission, Absorption, and Microscopy, McGraw-Hill, New York, 1967, pp. 17–25.
[23] X.W. Sun, H.S. Kwok, J. Appl. Phys. 86 (1999) 408.
[24] A.A. Dakhel, Appl. Phys. A 77 (2003) 677.
[25] D. Jia, L. Lu, W.M. Yen, Opt. Commun. 212 (2002) 97.
[26] S.M. Sze, Physics of Semiconductor Devices, 2nd ed., Wiley, 1981.
[27] V. Mikhelashvili, G. Eisenstein, F. Edelmann, J. Appl. Phys. 90 (2001) 5447.
[28] H.-C. Li, W. Si, A.D. West, X.X. Xi, Appl. Phys. Lett. 73 (1998) 464.
[29] K. Wandelt, C.R. Brundle, Surf. Sci. 157 (1985) 162.
[30] D.A. Neamen, Semiconductor Physics and Devices-Basic Principles, 2nd ed., Irwin-McGraw-Hill Comp, USA, Inc., 1997.

[31] W.H. Hill, Solid State Electron. 23 (1980) 987.
[32] A. Ghosh, Phys. Rev. B 41 (1990) 1479.
[33] S.R. Elliott, Adv. Phys. 36 (1987) 135.
[34] A.R. Long, Adv. Phys. 31 (1982) 553.
[35] S.R. Elliott, Phil. Mag. 36 (1977) 1291.
[36] R. Salam, Phys. Stat. Sol. (a) 117 (1990) 535.
[37] M. Pollak, T.H. Geballe, Phys. Rev. B 122 (1961) 1742.
[38] A. Vasudevan, S. Carin, M.A. Melloch, S. Harmon, Appl. Phys. Lett. 73 (1998) 671.
[39] A. Mansingh, R.P. Tandon, J.K. Vaid, J. Phys. Chem. Solids 36 (1975) 1267.
[40] K.K. Srivastava, A. Kumar, O.S. Panwar, L.N. Lakshminarayan, J. Non-Cryst. Solids 33 (1979) 205.
[41] M.A.M. Seyam, Appl. Surf. Sci. 181 (2001) 128.
[42] W.R. Harrell, J. Frey, Thin Solid Films 352 (1999) 195.
[43] M.A. Lampert, P. Mark, Current Injection in Solids, Academic Press, NY, 1970.
[44] A. Rose, Phys. Rev. 97 (1955) 1538.
[45] A.O. Oduor, R.D. Gould, Thin Solid Films 317 (1998) 409.

[46] A.M. Saleh, A.K. Hassan, R.D. Gould, J. Phys. Chem. Solids 64 (2003) 1297.
[47] M.A. Lampert, Rep. Prog. Phys. 27 (1964) 329.
[48] S.A. Awan, R.D. Gould, S. Gravano, Thin Solid Films 355–356 (1999) 456.
[49] R.D. Gould, M.S. Rahman, J. Phys. D 14 (1981) 79.
[50] Ya.G. Fedorenko, L.A. Otavina, S.V. Korenyuk, Tech. Phys. Lett. 26 (2000) 916.
[51] S.A. Awan, R.D. Gould, Thin Solid Films 423 (2003) 267.
[52] N. Kazuo, Infrared and Raman Spectra of Inorganic and Coordination Compounds, Part B, 5th ed., Wiley, 1997.
[53] M. Benmoussa, E. Ibnouelghazi, A. Bennouna, E.L. Ameziane, Thin Solid Films 265 (1995) 22.
[54] M.D. Stamate, Thin Solid Films 372 (2000) 246.
[55] A.A. Dakhel, Eur. Phys. J. AP (2004), available on line.
[56] A. Gracia-Murillo, C.L. Luyer, C. Garapon, C. Dujardin, E. Bernstein, C. Pedrini, J. Mugnier, Opt. Mater. 19 (2002) 161.
[57] W. Weng, J. Yang, Z. Ding, J. Non-Cryst. Solids 169 (1994) 177.
[58] M.W. Urban, B.C. Cornilsen, J. Phys. Chem. Solids 48 (1987) 479.